International Journal of Fluid Machinery and Systems
Vol. 2, No. 3, July-September 2009

Original Paper

Rotating Choke and Choked Surge in an Axial Pump Impeller

Toshifumi Watanabe [1], Hideyoshi Sato [2], Yasuhiko Henmi [2]
Hironori Horiguchi [1], Yutaka Kawata [3], and Yoshinobu Tsujimoto [1]

[1] Graduate School of Engineering Science, Osaka University
1-3 Machikaneyama, Toyonaka, Osaka, 560-8531, Japan
[2] Yamaha Motor Co., Ltd.
1400 Nippashi, Minami-ku, Hamamatsu, Shizuoka, 432-8528, Japan
[3] Faculty of Engineering, Osaka Institute of Technology
5-16-1 Omiya, Asahi-ku, Osaka, 535-8585, Japan

Abstract

Unlike usual turbopump inducers, the axial flow pump tested operates very stably at design flow rate without rotating cavitation nor cavitation surge. Flow visualization suggests that this is because the tip cavity smoothly extends into the flow passage without the interaction with the leading edge of the next blade. However, at low flow rate and low cavitation number, choked surge and rotating choke were observed. Their correlation with the performance curve under cavitation is discussed and their instantaneous flow fields are shown.

Keywords: Pump, Cavitation, Cavitation Instability, Rotating Choke, Choked Surge

1. Introduction

Turbopump inducers for rocket engines are used to suppress the head breakdown of the main impeller due to cavitation. Inducers operate with cavitation and it becomes unstable [1-4] in a certain operating condition and causes the shaft vibration. Cavitation surge [1] and rotating cavitation [2] [3] occur at the cavitation number above head breakdown. Recently, similar phenomena were observed under head breakdown. They are called "rotating choke" [5] [6] and "choked surge" [7] since the head breakdown is caused by choke and the cause of the instability is the positive slope of the performance curve due to choke.

The present paper reports about the rotating choke and the choked surge observed in an axial flow pump impeller with the geometry similar to the inducers for rocket engines. The rotating choke and the choked surge are observed in the same impeller for the first time. The visual observation of rotating choke was made for the first time. It is discussed why normal rotating cavitation did not occur in the pump tested.

2. Experiment

Figure 1 shows the cavitation tunnel used for the present study. The working fluid is deaerated water at ordinary temperatures. A water tank locates at the upstream of the impeller and the cavitation number σ is adjusted by changing the pressure of the air in the upper part of the tank using a vacuum pump. The flow rate ϕ is controlled by the butterfly valve located downstream of the impeller. The rotor is driven by an inverter motor through a torque meter. During the operation of the pump, the flow rate, the pressures at the inlet and outlet of the impeller, the fluctuating pressure at the inlet, the torque, the water temperature, and the rotational speed of the impeller are transferred to a computer through an A/D converter (National Instruments, PCI 6224). These values are displayed in a monitor for monitoring the condition of the operation by a software (National Instruments, LabVIEW8.0) and recorded.

Figure 2 shows the meridional cross section around the impeller. The inlet pressure p_1 is measured at the distance of 299mm ($z/D_T = -1.934$) upstream from the leading edge at tip. The outlet pressure p_2 is measured at 70mm ($z/D_T = 0.453$) downstream from the tip of the leading edge. The casing around the impeller is made of a transparent acrylic resin for visualizing the cavitation.

Figure 3 shows the geometry of the impeller. The diameter of the impeller is 154.6mm, the number of blades is 3, and the inlet and outlet blade angles at the tip are 11deg and 21deg, respectively. The solidity at the tip is about 1.17 and the tip clearance is

Received June 17 2009; accepted for publication August 6 2009: Review conducted by Prof. Wang Leqing. (Paper number O09020)
Corresponding author: Hironori Horiguchi, Associate Professor, horiguti@me.es.osaka-u.ac.jp

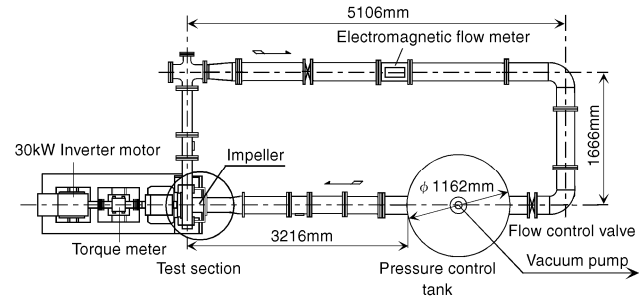

(a) Top view

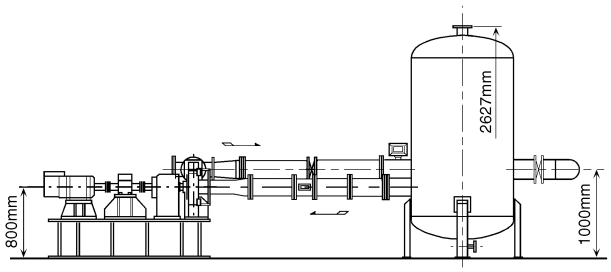

(b) Side view

Fig. 1 Cavitation tunnel

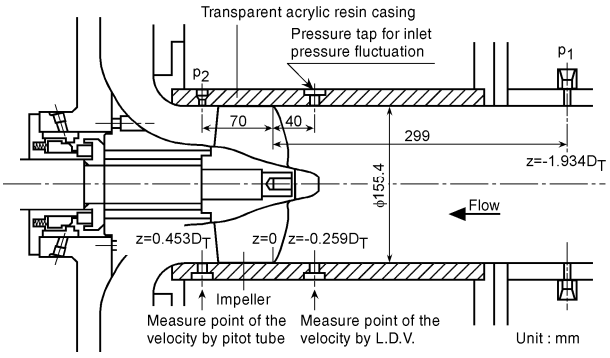

Fig. 2 Meridian cross section of the test section

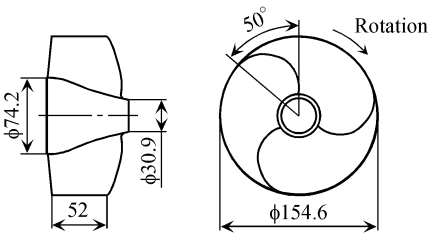

Fig. 3 Geometry of the impeller

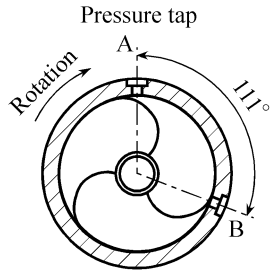

Fig. 4 Circumferential position of the pressure taps

0.4mm. The impeller has a swept back leading edge and the sweep angle is about 50deg. The flow rate near the maximum efficiency point $\phi_0 = 0.180$ was defined as the reference flow coefficient.

In the measurement of the flow coefficient ϕ, the pressure coefficient ψ, and the power coefficient τ for the performance curve, the rotational speed of the impeller was set 1500rpm to avoid cavitation. In the non-cavitating flow, time-averaged velocities were measured by LDV at the distance of 40mm ($z/D_T = -0.259$) upstream from the tip of the leading edge and by an one hole pitot tube at the distance of 70mm ($z/D_T = 0.453$) downstream from the tip of the leading edge.

The measurement of the suction performance curve was made by decreasing the tank pressure from atmospheric pressure. The rotational speed of the impeller was 2200rpm. The inlet fluctuating pressure at $z/D_T = -0.264$ was measured by pressure transducers (Kyowa, PGMC-A-1MP) flush mounted on the casing. To identify the mode of oscillations, the pressure transducers were installed at two circumferential locations as shown in Fig.4. Spectrum analysis for the pressure signals was performed by a FFT analyzer.

Based on the results of the spectrum analysis, the cavitation instabilities were identified. Pictures were taken by a high speed video camera with the frame rate of 4500frames/sec.

3. Results and Discussions

3.1 Performance Curve

Figure 5 shows the non-cavitating performance curve at 1500rpm. Figure 5(a) shows the pressure coefficient ψ in which the inlet pressure p_1 was estimated by subtracting the dynamic pressure and the pressure loss in the suction pipe from the total pressure in the tank, and shows the pump efficiency η. Figure 5(b) shows the values of ψ and η based on p_1 measured at $z/D_T = -1.934$. The values of η was evaluated using the static pressure at the inlet and outlet. In Fig.5(a), the values of ψ is larger than those of Fig.5(b) in $\phi < 0.08$. This difference was caused by the increase of measured p_1 in Fig.5(b) due to the centrifugal force on the swirling backflow which covers the pressure transducer at lower flow rates. Since the backflow reaches the upstream end of the transparent casing at $\phi = 0.108$, it is quite possible that the backflow reaches at the measuring point of p_1 at $\phi = 0.08$. Although we have larger scatter in $\phi < 0.08$ for both cases, the performance curve shown in Fig.5(b) is much smoother. So, the increase of ψ in Fig.5(a) in $\phi < 0.08$ is considered to be caused by the pressure rise due to the centrifugal force on the swirling backflow at the inlet.

In order to determine the change of flow pattern at low flow rate, the velocity distribution was measured at the inlet ($z/D_T = -0.259$) and the outlet ($z/D_T = 0.453$). The backflow started to occur at the inlet at $\phi = 0.090$. The size of the backflow and its velocity did not change largely at ϕ=0.08. At the outlet, the backflow at hub started to occur at $\phi = 0.108$. Although the size of the backflow increased gradually as the flow rate decreased, it did not change drastically near $\phi = 0.08$.

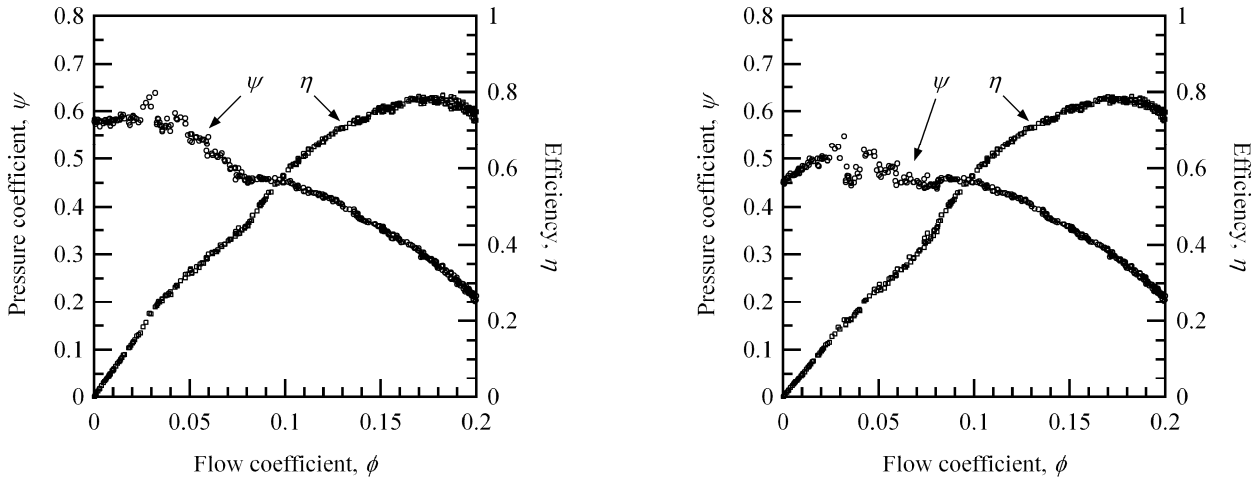

(a) p_1 is estimated from tank pressure

(b) p_1 is measured

Fig. 5 Performance curve at 1500rpm

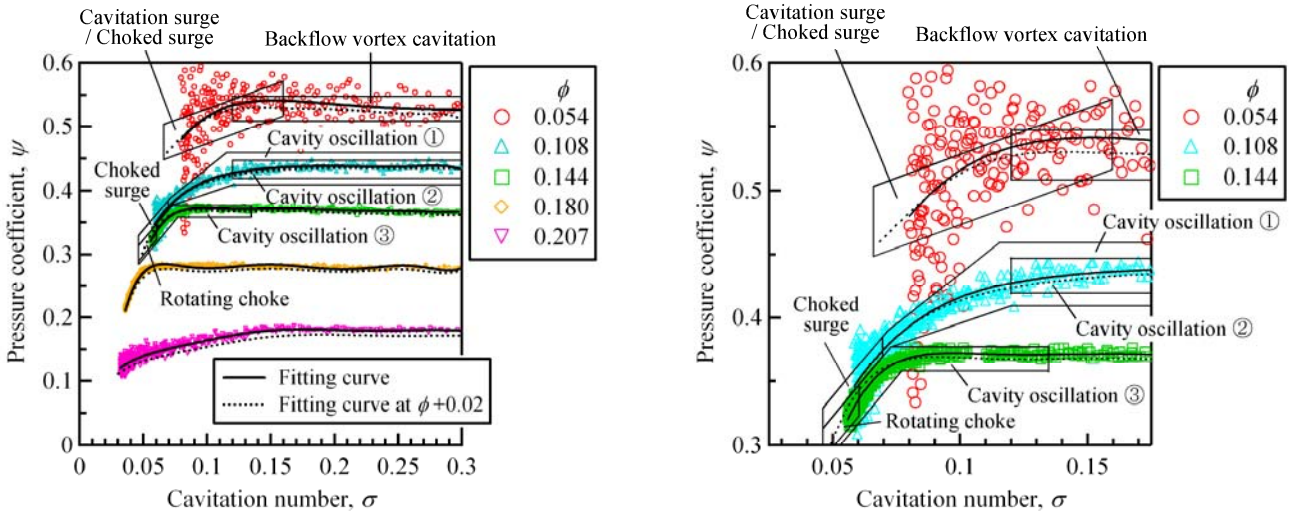

(a) Suction performance

(b) Detail of Fig.6(a)

Fig. 6 Suction performance curves with the occurrence regions of cavitation instabilities at 2200rpm

3.2 Suction Performance

Figure 6 shows the suction performance curves where the estimated inlet pressure p_1 was used for ψ and σ. Figure 6(b) shows the magnified figure of the left upper part of Fig.6(a). The fitted suction performance curves at various flow coefficients are shown by full lines.

To examine the slope of $\phi-\psi$ curves, the suction performance was measured also at slightly (by 0.02) larger flow rate than each flow rate and their fitting curves are shown by dotted curves. In most cases, the head is smaller at larger flow coefficient, showing negative slope of performance curve. However, at low flow coefficient and low cavitation number where the head is decreased, the head at larger flow coefficient becomes identical to or larger than that at slightly larger flow rate. In these cases, the slope of ϕ-ψ curve becomes zero or positive.

Figure 7 shows the spectrum of the inlet pressure fluctuation measured at $z/D_T = -0.259$. The value of θ in Fig.7 shows the phase of the pressure fluctuation at the point B in Fig.4 from that at the point A. Negative value of θ means the phase delay and represents that the disturbance propagates in the rotational direction of the impeller. $\theta = -111$deg means the disturbance with one cell which propagates in the rotational direction of the impeller. Based on the spectrum of the inlet pressure fluctuation, the occurrence regions of the cavitation instabilities are shown in the suction performance curve in Fig.6. In the region where the slope of $\phi-\psi$ curve is positive or 0, the rotating choke or choked surge occur. We should note that no cavitation instability occurs at the reference flow rate $\phi = 0.180$. This shows that the pump tested is quite stable as compared with inducers for rocket engines. At the larger flow rate $\phi = 0.207$, the cavity occurs on the pressure surface and the values of ψ decreases gradually from the larger σ as the values of σ decreases.

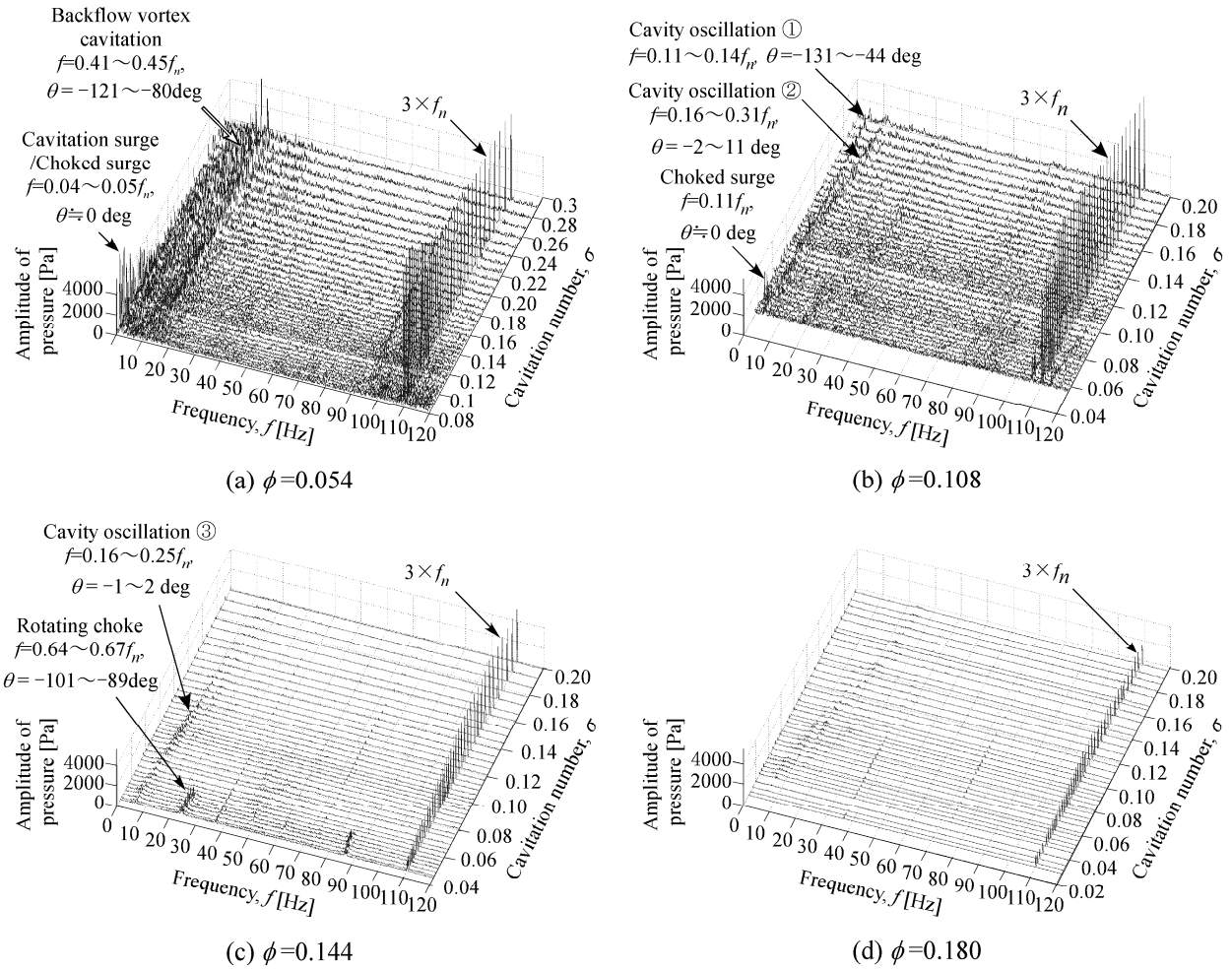

(a) ϕ=0.054 (b) ϕ=0.108

(c) ϕ=0.144 (d) ϕ=0.180

Fig. 7 Spectra of the inlet pressure fluctuation at various flow coefficients at 2200rpm

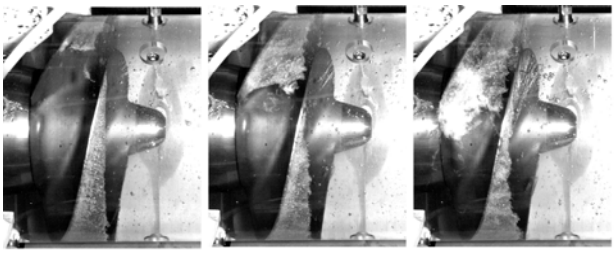

(a) σ=0.06 (b) σ=0.04 (c) σ=0.03

Fig. 8 Pictures of the cavity at ϕ=0.180, 2200rpm

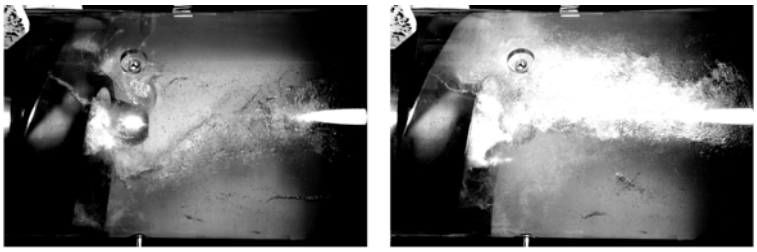

(a) σ=0.22 (b) σ=0.16

Fig. 9 Pictures of the backflow vortex cavity at ϕ=0.054, 2200rpm

3.3 Cavitation at the Reference Flow Rate

The cavitation instabilities did not occur at the reference flow rate. As shown in Fig.8(a), at $\sigma = 0.06$ where the head breakdown does not occur, the blade surface cavity and the backflow vortex cavity do not exist and thin tip leakage cavity extends towards the throat as the value of σ decreases without the interaction with the leading edge of the neighboring blade. When the tip leakage cavity reaches the throat as shown in Fig.8(b), the blade surface cavity develops. As the value of σ decreases further, the tip leakage cavity extends to the blade passage as shown in Fig.8(c), and the head breakdown occurs.

The smooth extension of thin tip leakage cavity towards the blade passage without the interaction with the leading edge is the cause of stable operation without rotating cavitation.

3.4 Backflow Vortex Cavitation

The backflow vortex cavitation started to occur at $\phi = 0.144$ and its axial length became $0.5 \sim 1.0 D_T$ at $\phi = 0.108$. The number of the backflow vortex cavity was more than 3 at these flow rates, and the effect of the backflow vortex cavitation could not be recognized clearly in the spectrum shown in Fig.7. Figure 9 shows the pictures of the cavity at $\phi = 0.054$. One large vortex cavity extends upstream. The spectrum indicated by "Backflow vortex cavitation" in Fig.7(a) for $\phi = 0.054$ has the phase

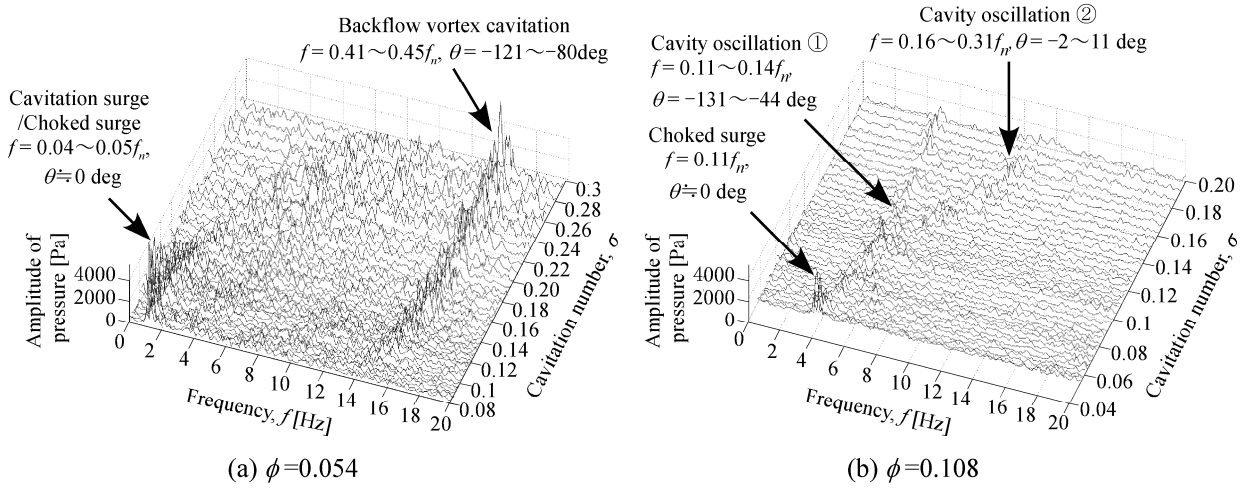

(a) ϕ=0.054 (b) ϕ=0.108

Fig. 10 Details of Figs.7(a) and (b)

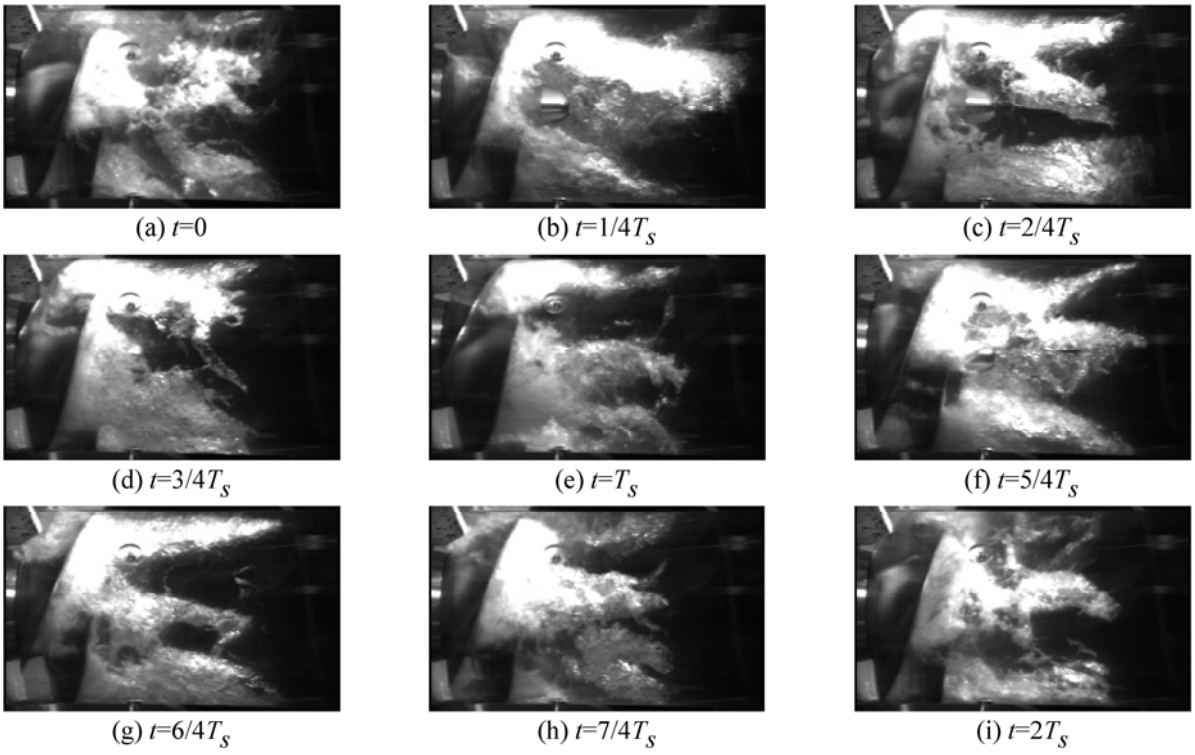

(a) t=0 (b) $t=1/4T_S$ (c) $t=2/4T_S$

(d) $t=3/4T_S$ (e) $t=T_S$ (f) $t=5/4T_S$

(g) $t=6/4T_S$ (h) $t=7/4T_S$ (i) $t=2T_S$

Fig. 11 Pictures of the cavity in the chocked surge at ϕ=0.108, σ=0.06, 2200rpm, T_s=0.29sec (3.5Hz)

angles of $-121\sim-80$deg and it is thought to be caused by the rotation of the backflow vortex cavity with the frequency of $41\sim45\%$ of the impeller's rotational frequency. Figure 10(a) shows the magnified figure of Fig.7(a). The amplitude of the spectrum due to the backflow vortex cavity decreases as the cavitation number decreases. This is because the center of the backflow vortex gets closer to the center of the inlet pipe, as shown in Fig.9.

3.5 Cavitation Surge and Choked Surge

As shown in Fig.7(a) and Fig.10(a) for $\phi=0.054$, a component with $\theta\approx0$deg and $f/f_n=0.04\sim0.05$ appears. The suction performance curves in Fig.6(b) shows that the negative slope of the performance curve decreases as the cavitation number is decreased. Figure 10(a) shows that the amplitude of this component increases as the decrease of cavitation number. So, it is possible to consider that a normal cavitation surge is switching to choked surge. If we plot the suction performance curve using measured p_1, the region with positive slope will become larger.

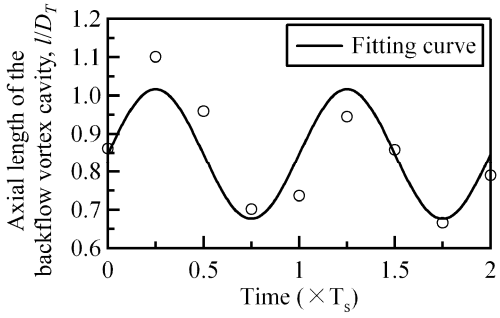

Fig. 12 Axial length of the backflow vortex cavity in the choked surge at ϕ=0.108, σ=0.06, 2200rpm

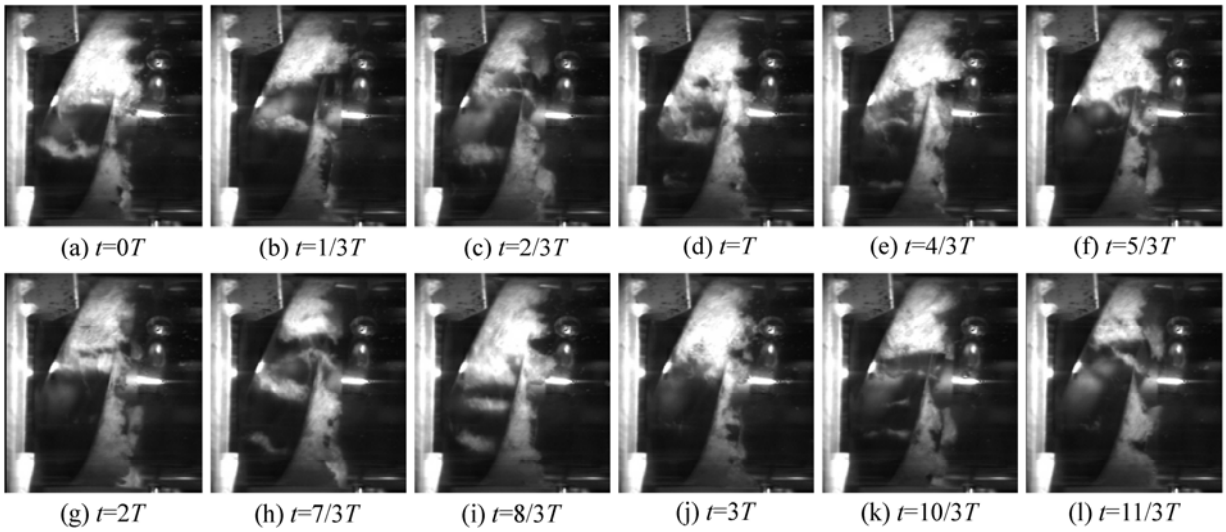

Fig. 13 Pictures of the cavity in the rotating choke at ϕ=0.144, σ=0.058, 2200rpm, T=0.027sec (36.7Hz=f_n)

3.6 Choked Surge

In Fig.7(b) and Fig.10(b), a spectrum with $\theta \approx 0\,\mathrm{deg}$ and $f / f_n = 0.11$ is observed at $\phi = 0.108$ in $\sigma < 0.07$. This component is due to the choked surge because the head breakdown occurs at $\phi = 0.108$ in $\sigma < 0.07$ as shown in Fig.6 and the slope of $\phi - \psi$ curve is 0. Figure 11 shows the pictures from high speed video. The pictures with two periods $2T_s$ of the choked surge are shown. The tip cavity nearly reaches the throat. This supports the identification as a choked surge. However, the length of backflow vortex cavity is also oscillating, as plotted in Fig.12. This suggests the possibility of cavitation surge associated with backflow cavitation [8] which usually occurs above head breakdown. In the reference [7], the choked surge was so severe that the cavity extended to the blade trailing edge. Comparing with this, the choked surge in the present study was mild.

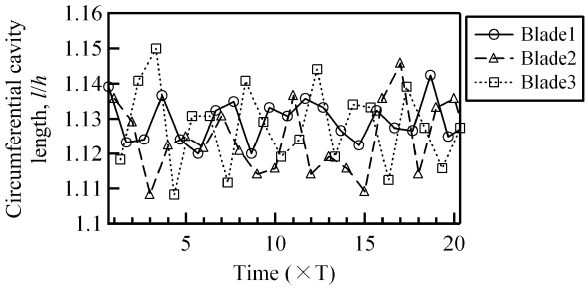

Fig. 14 Circumferential cavity length under rotating choke at ϕ=0.144, σ=0.058, 2200rpm

3.7 Rotating Choke

The spectrum with $f / f_n = 0.64 \sim 0.67$ and $\theta = -101 \sim -89\,\mathrm{deg}$ is observed at $\phi = 0.144$ in $\sigma < 0.06$, as shown in Fig.7(c). In Fig.6, the slope of $\phi - \psi$ curve is positive at $\phi = 0.144$ in $\sigma < 0.06$. Although the angle θ of $-101 \sim -89\,\mathrm{deg}$ is a little different from the angle $-111\,\mathrm{deg}$ between the pressure transducers, we consider that the components with $f / f_n = 0.64 \sim 0.67$ is due to the rotating choke. Pictures at every 1/3 rotation of the impeller are shown in Fig.13, where T is the period of the impeller rotation. After one revolution of the impeller, larger cavities shown in Figs.13(a), (e), (i), (j) move to the next blade in the opposite direction of the impeller rotation. The propagation velocity ratio defined as (the rotational velocity of the cavity in a stationary frame)/(the rotational velocity of the impeller) is 2/3=0.66 and agrees with the observed frequency ratio of $f / f_n = 0.64 \sim 0.67$. Figure 14 shows the circumferential cavity length l normalized by the circumferential pitch h of the blades. The cavity propagates in the order of Blade 1, 2, 3, although the propagation is not regular. The length of the cavity on a certain blade becomes maximum or minimum about 7 times during 20 revolutions and (20-7)/20=0.65 agrees with the observed frequency ratio $f / f_n = 0.64 \sim 0.67$.

Figure 13 also shows that the tip cavity extends into the blade passage and chokes the passage. Figure 13(i) shows that the backflow vortices are cut by the blade and flowing down the passage. This also shows that the irregular upstream boundary of the tip cavity is caused by backflow vortices.

3.8 Other Spectral Components

In addition to the spectral components due to the cavitation instabilities mentioned above, the components of No.1 ~ 3 with smaller frequency and amplitude were observed as shown in Figs.6 and 7. The components of No.2 and 3 with the smaller phase angle are due to the oscillation of the surge mode. The spectrum of No.1 with the larger phase angle is due to the oscillation of the rotational mode. These modes could not be studied further because the amplitudes were too small.

4. Conclusions

The performance test of an axial pump impeller was carried out. The results can be summarized as follows.

(1) No cavitation instability was found at design flow rate. This is caused by smooth extension of thin tip cavity into the blade

passage.
(2) At the lower flow rate and cavitation number, both rotating choke and the choked surge were observed.
(3) Rotating choke and choked surge are correlated with the positive slope of ϕ-ψ performance.
(4) Visual observations of rotating choke and choked surge were made.

It is favorable to provide the conditions for the occurrence of rotating choke and choked surge. However, the correlation between the design and their occurrence has been left for future study.

Acknowledgement

The authors would like to thank undergraduate student Yusuke Arimoto for his cooperation of the experiment.

Nomenclature

A	Area of the cross section of the casing [m^2]	T_s	Period of the choked surge [s]
D_T	Diameter of the impeller [m]	v	Flow velocity [m/s]
f	Frequency [Hz]	v_1	Mean axial velocity in the casing at the upstream of the impeller $= Q / A$ [m/s]
f_n	Frequency of the impeller rotation [Hz]		
h	Blade spacing at the tip [m]	z	Axial coordinate from the tip of the leading edge [m]
l	Cavity length [m]		
p_1	Pressure at the inlet [Pa]	ϕ	Flow coefficient $= v_1 / U_T$
p_2	Pressure at the outlet [Pa]	ϕ_0	Reference flow coefficient $= 0.180$
p_v	Vapor pressure [Pa]	η	Pump efficiency $= \phi\psi / (2\tau)$
Q	Volume flow rate [m^3/s]	θ	Phase of the pressure fluctuation
R_T	Radius of the impeller [m]	ρ	Density of fluid [kg/m^3]
U_T	Tip speed of the impeller [m/s] $= \pi D_T f_n$	σ	Cavitation number $= (p_1 - p_v) / (\rho U_T^2 / 2)$
t	Time [s]	τ	Power coefficient $= T\omega / (\rho U_T^3 A)$
T	Torque [N·m], or the period of the impeller rotation [s]	ω	Angular velocity of the impeller [rad/s]
		ψ	Pressure coefficient $= (p_2 - p_1) / (\rho U_T^2 / 2)$

References

[1]Young, W. E., Murphy, R., and Reddecliff, J. M., 1972, “Study of Cavitating Inducer Instabilities,” Final Report, NACA-CR-123939, pp.1-149.
[2]Kamijo, K., Shimura, T., and Watanabe, M., 1977, “An Experimental Investigation of Cavitating Inducer Instability,” ASME Paper, 77-WA/FW-14, pp.1-9.
[3]Tsujimoto, Y., Kamijo, K., and Yoshida, Y., 1993, “A Theoretical Analysis of Rotating Cavitation in Inducers,” Transactions of the ASME, Journal of Fluids Engineering, Vol.115, No.1, pp.135-141.
[4]Tsujimoto, Y., Watanabe S., and Horiguchi, H., 2008, “Cavitation Instabilities of Hydrofoils and Cascades,” International Journal of Fluid Machinery and Systems, Vol.1, No.1, pp.38-46.
[5]Shimura, T., Yoshida, M., Kamijo, K., Uchiumi, M., and Yasutomi, Y., 2002, “A Rotating Stall Type Phenomenon Caused by Cavitation in LE-7A LH2 Turbopump,” JSME International Journal, Series B, Vol.45, No.1, pp.41-46.
[6]Semenov, Y., Fujii, A., and Tsujimoto, Y., 2004, “Rotating Choke in Cavitating Turbopump Inducer,” Transactions of the ASME, Journal of Fluids Engineering, Vol.126, No.1, pp.87-93.
[7]Watanabe, T., Kang, D., Cervone, A., Kawata, Y., and Tsujimoto, 2008, Y., “Choked Surge in a Cavitating Turbopump Inducer,” International Journal of Fluid Machinery and Systems, Vol.1, No.1, pp.64-75.
[8]Yamamoto, K. and Tsujimoto, Y., 2009, “Backflow Vortex Cavitation and Its Effects on Cavitation Instabilities,” International Journal of Fluid Machinery and Systems,” Vol.2, No.1, pp.40-54.